arXiv:0709.0616v1 [gr-qc] 5 Sep 2007

Vacuum shell in the Schwarzschild-de Sitter world

S V Chernov[†‡] **and V I Dokuchaev**[†]

† Institute for Nuclear Research of the Russian Academy of Sciences
60th October Anniversary Prospect 7a, 117312 Moscow, Russia
‡ Moscow Institute of Physics and Technology
Dolgoprudny, 141700 Moscow region, Russia

E-mail: `chernov.s@mail.ru, dokuchaev@inr.npd.ac.ru`

Abstract. We construct the classification scheme for all possible evolution scenarios and find the corresponding global geometries for dynamics of a thin spherical vacuum shell in the Schwarzschild-de Sitter metric. This configuration is suitable for the modelling of vacuum bubbles arising during cosmological phase transitions in the early Universe. The distinctive final types of evolution from the local point of view of a rather distant observer are either the unlimited expansion of the shell or its contraction with a formation of black hole (with a central singularity) or wormhole (with a baby universe in interior).

PACS numbers: 04.20.-q,04.70.-s,98.80.-k

1. Introduction

One of the promising mechanisms of primordial black holes and wormholes formation is a collapse of vacuum bubbles during phase transitions in the early Universe [1, 2, 3, 4, 5]. The supermassive black holes in the centers of galaxies may be also originated by this mechanism. We will describe the possible types of dynamical evolution of vacuum bubbles in the Schwarzschild-de Sitter metric by using the thin shell approximation for the boundary between the true and false vacuum. The formalism of thin shells in General Relativity was first developed by W. Israel [6]. Later this formalism was elaborated and adjusted for the case of cosmological vacuum phase transitions [7, 8, 9, 10].

The boundary of vacuum bubble divides the Schwarzschild-de Sitter space-time into internal and external regions. In the following these regions are designated by indexes "*in*" and "*out*" respectively. Our aim is a full classification of possible evolution scenarios of vacuum bubbles versus of parameters of the Schwarzschild-de Sitter space-time and initial conditions for a thin shell. It appears that a useful classification quantity for this problem is a mass parameter m which will be defined below. Depending on this mass parameters the bubble is either expanding to infinity or contracting with a final formation of black hole or wormhole [11, 12, 13]. This work is a generalization of the earlier analysis in [14, 15, 16, 17], where only some particular scenarios for this problem were investigated.

In previous works [10, 11, 12, 14, 15, 18, 19] were considered only the particular cases of solutions corresponding to the zero value of our inner mass parameter $m_{in} = 0$. We describe a more general case when $m_{in} \neq 0$, and then the new types of solutions appear. The bubbles are originated in the phase transition in the early universe and may contain in principle smaller bubbles inside (see e. g. [11, 12]). To model this in a formal way we include an interior mass parameter m_{in}. This parameter may be considered as a seed black hole.

In general, solutions with $m_{in} \neq 0$ are quite the similar ones to considered in [10, 11, 12, 14, 15, 18, 19]. At the same time the addition of inner mass parameter m_{in} results in a complication of the classification scheme for possible solutions.

In Section 2 the equation of motion for a thin shell in the Schwarzschild-de Sitter metric is analyzed. Basing on this equation in Section 3 we develop a classification scheme for possible evolution scenarios and construct also the Carter-Penrose diagrams for corresponding global geometries. The concluding remarks are shortly summarized in Section 4.

2. Equation of motion

The Schwarzschild-de Sitter metric can be written in the form

$$ds^2 = \left(1 - \frac{2M}{r} - \frac{8\pi}{3}\varepsilon r^2\right) dt^2 - \left(1 - \frac{2M}{r} - \frac{8\pi}{3}\varepsilon r^2\right)^{-1} dr^2 - r^2 d\Omega, \quad (1)$$

where M is the Schwarzschild mass, ε is a vacuum energy density and $d\Omega = d\theta^2 + \sin^2\theta\, d\phi^2$. This metric has the following specific properties. The positive roots of equation

$$1 - \frac{2M}{r} - \frac{8\pi\varepsilon}{3} r^2 = 0 \tag{2}$$

define the radii of event horizons in this metric. The number of positive roots (and so the number of event horizons) depends on the ratio of M and $1/\sqrt{\varepsilon}$. There are no event horizons, if $M > m_2 = 1/\sqrt{72\pi\varepsilon}$. There is only one event horizon, $r_{\rm h1} = 1/\sqrt{8\pi\varepsilon}$, if $M = m_2$. In the case $M < m_2$ there are two distinctive event horizons:

$$r_{\rm h2} = 2\sqrt{\frac{p}{3}} \cos\left[\frac{\pi}{3} + \frac{1}{3}\arctan\sqrt{\frac{4p^3}{27q^2} - 1}\right]; \tag{3}$$

$$r_{\rm h3} = 2\sqrt{\frac{p}{3}} \cos\left[\frac{\pi}{3} - \frac{1}{3}\arctan\sqrt{\frac{4p^3}{27q^2} - 1}\right], \tag{4}$$

where $p = 3/(8\pi\varepsilon)$ and $q = 3M/(4\pi\varepsilon)$. It can be shown that $r_{\rm h2} < r_{\rm h1} < r_{\rm h3} < \sqrt{3} r_{\rm h1}$. See in the Fig. 1 the corresponding Carter-Penrose diagrams for global geometry of the Schwarzschild-de Sitter space-time [9, 15].

The basic equation of motion for a thin vacuum shell in the Schwarzschild-de Sitter space-time, resulting from the matching of the inner and outer metrics on the shell, can be written in the following form [7, 8, 10, 16, 20, 21, 22, 23]:

$$4\pi\sigma\rho = \sigma_{\rm in}\sqrt{\dot\rho^2 + 1 - \frac{8\pi}{3}\varepsilon_{\rm in}\rho^2 - \frac{2m_{\rm in}}{\rho}} - \sigma_{\rm out}\sqrt{\dot\rho^2 + 1 - \frac{8\pi}{3}\varepsilon_{\rm out}\rho^2 - \frac{2m_{\rm out}}{\rho}}. \tag{5}$$

In this equation $\rho = \rho(\tau)$ is a shell radius, τ is a proper time measured by an observer at rest with respect to this shell, $\dot\rho$ is derivative with respect to a proper time, σ is a surface energy density on the shell (in the discussed vacuum case σ=const), $m_{\rm in}$ and $m_{\rm out}$ is the Schwarzschild mass of the inner and outer region respectively, $\varepsilon_{\rm in}$ is an energy density of the inner region, $\varepsilon_{\rm out}$ is an energy density of the outer region and symbols $\sigma_{\rm in,out} = \pm 1$. These symbols equal to 1, if radius of a two-dimensional sphere is growing in the direction of an outgoing normal, and equal to -1 in the opposite case.

For a further analysis we rewrite the equation of motion (5) in the "energy conservation" form $(1/2)\dot\rho^2 + U(\rho) = 0$, with an effective potential

$$U(\rho) = \frac{1}{2} - \frac{(m_{\rm out} - m_{\rm in})^2}{32\pi^2\sigma^2\rho^4} - \frac{m_{\rm out} + m_{\rm in}}{2\rho} - (m_{\rm out} - m_{\rm in})\frac{\varepsilon_{\rm out} - \varepsilon_{\rm in}}{12\pi\sigma^2\rho}$$
$$- \frac{(\varepsilon_{\rm in} + \varepsilon_{\rm out} + 6\pi\sigma^2)^2 - 4\varepsilon_{\rm in}\varepsilon_{\rm out}}{18\sigma^2}\rho^2, \tag{6}$$

which is shown in the Fig. 2. Values of σ_{in} and σ_{out} in the equation of motion (5) in the "energy conservation" form are defined by relations

$$\sigma_{\rm in} = \operatorname{sign}\left[m_{\rm out} - m_{\rm in} + \frac{4\pi}{3}(\varepsilon_{\rm out} - \varepsilon_{\rm in})\rho^3 + 8\pi^2\sigma^2\rho^3\right]; \tag{7}$$

$$\sigma_{\rm out} = \operatorname{sign}\left[m_{\rm out} - m_{\rm in} + \frac{4\pi}{3}(\varepsilon_{\rm out} - \varepsilon_{\rm in})\rho^3 - 8\pi^2\sigma^2\rho^3\right]. \tag{8}$$

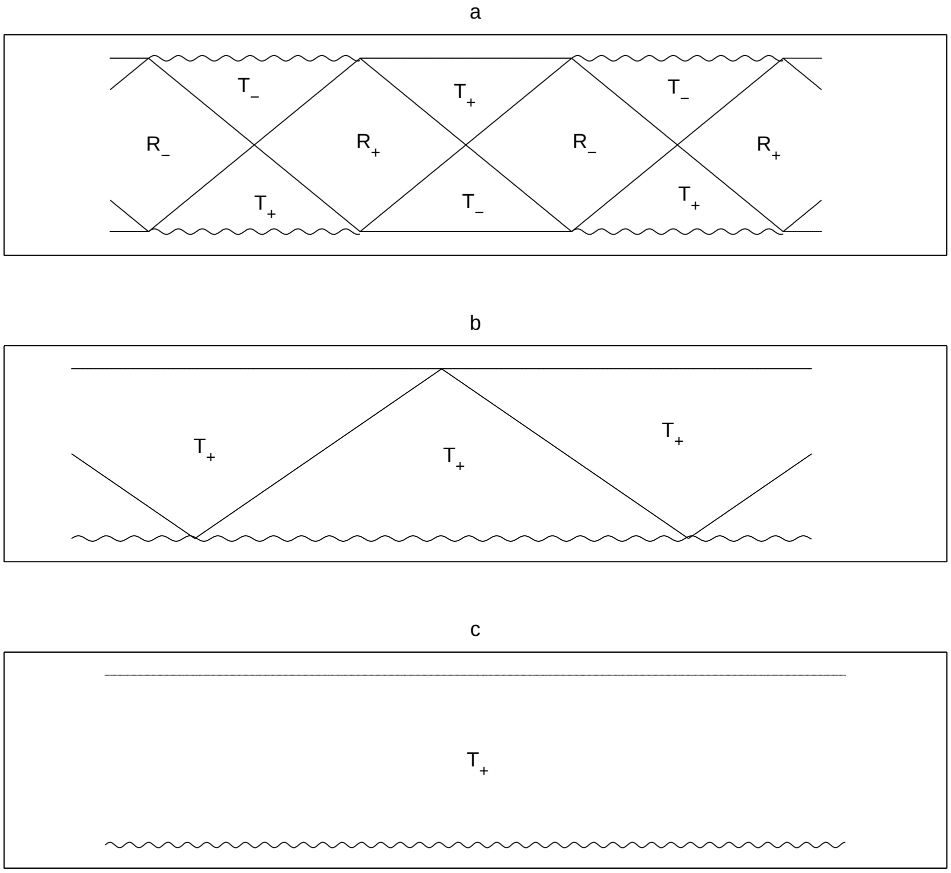

Figure 1. The Carter-Penrose diagrams for the Schwarzschild-de Sitter metric. In the case (a), when $M < m_2$, there are event horizons. There is only one event horizon in the case (b), when $M = m_2$. In the case (c), when $M > m_2$, the event horizon is absent. Diagrams (b) and (c) are shown for the case of expansion. The regions T_+ and T_- and also zero and infinity lines are swapped in the corresponding (nonshown) diagrams for the case of contraction. The oppositely directed null lines in these diagrams and in the following ones are not necessarily perpendicular to each other due to arbitrary deformation of the coordinate systems.

We will consider the general case when a surface energy density of the shell σ may be as positive and negative. It must be noted that for the positive value of σ there is the exceptional case, when $\sigma_{\text{in}} = -1$ and $\sigma_{\text{out}} = 1$. In this case the equation of motion (5) has no solution. It would be also seen in the following Carter-Penrose diagrams.

It is useful to define the following two quantities, one with a dimension of mass, $m = m_{\text{out}} + m_{\text{in}}$, and one dimensionless, $\mu = (m_{\text{out}} - m_{\text{in}})/(m_{\text{out}} + m_{\text{in}})$. With this definitions it is seen from (7) that σ_{in} changes its sign at $\rho(\tau) = \rho_1$, where

$$\rho_1^3 = \frac{3\mu m}{4\pi(\varepsilon_{\text{in}} - \varepsilon_{\text{out}} - 6\pi\sigma^2)}, \tag{9}$$

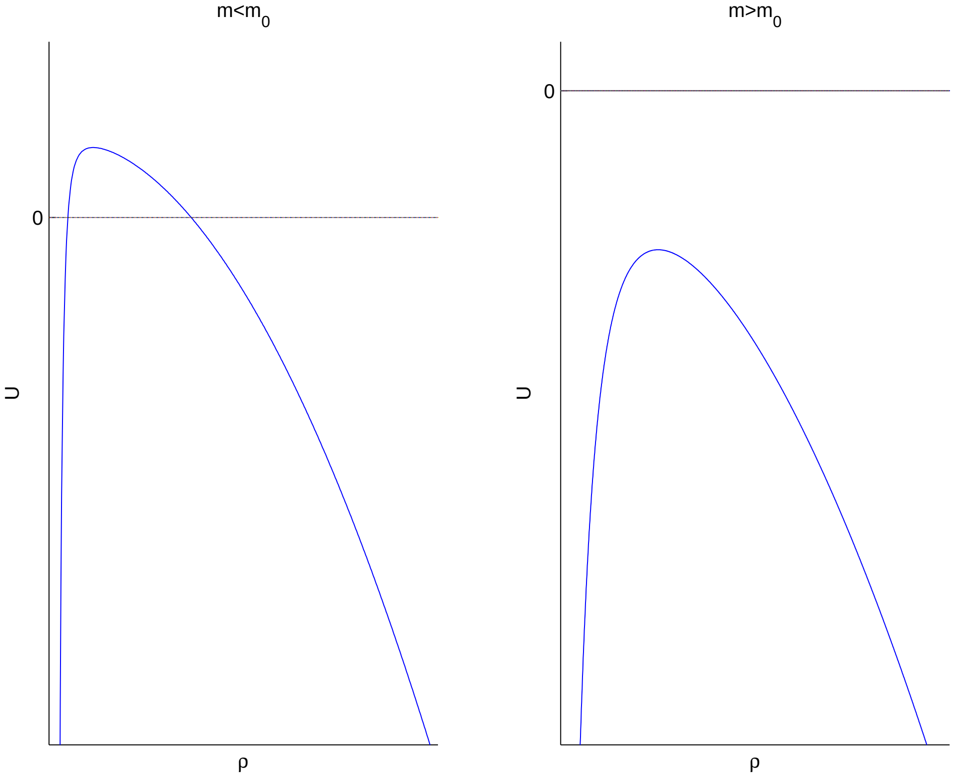

Figure 2. The graphs of potential function $U(\rho)$ from (6) at $m < m_0$ (left) and $m > m_0$ (right).

provided that (i) $\mu > 0$ and $\varepsilon_{\rm in} > \varepsilon_{\rm out} + 6\pi\sigma^2$ or (ii) $\mu < 0$ and $\varepsilon_{\rm in} < \varepsilon_{\rm out} + 6\pi\sigma^2$. Respectively, $\sigma_{\rm out}$ changes its sign when $\rho(\tau) = \rho_2$, where

$$\rho_2^3 = \frac{3\mu m}{4\pi(\varepsilon_{\rm in} - \varepsilon_{\rm out} + 6\pi\sigma^2)}, \tag{10}$$

provided, that (iii) $\mu > 0$ and $\varepsilon_{\rm in} > \varepsilon_{\rm out} - 6\pi\sigma^2$ or (iv) $\mu < 0$ and $\varepsilon_{\rm in} < \varepsilon_{\rm out} - 6\pi\sigma^2$.

Now we consider a behavior of the effective potential (6). The zeros of this potential, $U(\rho) = 0$, define the bounce points of solution when $\dot\rho = 0$. The maximum of potential (6) is at the point $\rho = \rho_{\rm max}$, where

$$\begin{aligned}\rho_{\rm max}^3 = my_{\rm max} = \frac{9\sigma^2}{4}m\Biggl\{1 + \mu\frac{\varepsilon_{\rm out} - \varepsilon_{\rm in}}{6\pi\sigma^2} \\ + \sqrt{\left(1+\mu\frac{\varepsilon_{\rm out} - \varepsilon_{\rm in}}{6\pi\sigma^2}\right)^2 + \frac{2\mu^2}{9\pi^2\sigma^4}[(\varepsilon_{\rm in} + \varepsilon_{\rm out} + 6\pi\sigma^2)^2 - 4\varepsilon_{\rm in}\varepsilon_{\rm out}]}\Biggr\} \\ \Bigg/ \; [(\varepsilon_{\rm in} + \varepsilon_{\rm out} + 6\pi\sigma^2)^2 - 4\varepsilon_{\rm in}\varepsilon_{\rm out}].\end{aligned} \tag{11}$$

This maximum corresponds to the zero of potential, $U(\rho_{\rm max}) = 0$, at $m = m_0$, where.

$$\begin{aligned}m_0 = \sqrt{y_{\rm max}}\Bigg/\Biggl\{1 + \frac{y_{\rm max}}{9\sigma^2}[(\varepsilon_{\rm in} + \varepsilon_{\rm out} + 6\pi\sigma^2)^2 - 4\varepsilon_{\rm in}\varepsilon_{\rm out}] \\ + \mu\frac{\varepsilon_{\rm out} - \varepsilon_{\rm in}}{6\pi\sigma^2} + \frac{\mu^2}{16\pi^2\sigma^2 y_{\rm max}}\Biggr\}^{3/2}.\end{aligned} \tag{12}$$

The potential $U(\rho_{\max}) > 0$ at $m < m_0$ and vise versa. A second derivative of the potential (6) is

$$\begin{aligned} \frac{d^2U}{d\rho^2} = &-\frac{m}{\rho^3} - \frac{4\pi(\varepsilon_{\rm out}+\varepsilon_{\rm in})+12\pi^2\sigma^2}{3} \\ &-\frac{9\mu^2m^2}{16\pi^2\sigma^2\rho^6} - \left(\frac{\varepsilon_{\rm out}-\varepsilon_{\rm in}}{3\sigma} + \frac{\mu m}{4\pi\sigma\rho^3}\right)^2 < 0. \end{aligned} \tag{13}$$

It is negative everywhere, and so there is no of a stable equilibrium point for the equation of motion (5).

At the next step let us define the values of parameter m when radii ρ_1 and ρ_2 (where $\sigma_{\rm in}$ and $\sigma_{\rm out}$ change the sign) coincide with the bounce points of the equation of motion (5). The corresponding solution of equation $U(\rho_1)=0$ is $m=m_1$, where

$$m_1 = \sqrt{\frac{3\mu}{4\pi(\varepsilon_{\rm in}-\varepsilon_{\rm out}-6\pi\sigma^2)\left(1+\mu\frac{\varepsilon_{\rm in}+\varepsilon_{\rm out}+6\pi\sigma^2}{\varepsilon_{\rm in}-\varepsilon_{\rm out}-6\pi\sigma^2}\right)^3}}. \tag{14}$$

Respectively, the corresponding solution of equation $U(\rho_2)=0$ is $m=m_3$, where

$$m_3 = \sqrt{\frac{3\mu}{4\pi(\varepsilon_{\rm in}-\varepsilon_{\rm out}+6\pi\sigma^2)\left(1+\mu\frac{\varepsilon_{\rm in}+\varepsilon_{\rm out}+6\pi\sigma^2}{\varepsilon_{\rm in}-\varepsilon_{\rm out}+6\pi\sigma^2}\right)^3}}. \tag{15}$$

By using (12), (14) and (15) it can be shown that both $m_1 < m_0$ and $m_3 < m_0$.

There are degenerate cases when the inner and outer regions with respect to the shell have only one event horizon. The inner Schwarzschild-de Sitter metric has only one event horizon when $m = m_{21}$, where

$$m_{21} = \frac{1}{(1-\mu)\sqrt{18\pi\varepsilon_{\rm in}}}. \tag{16}$$

Respectively, the outer Schwarzschild-de Sitter metric has only one event horizon when $m = m_{22}$, where

$$m_{22} = \frac{1}{(1+\mu)\sqrt{18\pi\varepsilon_{\rm out}}}. \tag{17}$$

It can be verified that both $m_{21} > m_0$ and $m_{22} > m_0$.

For the following analysis of the dynamical evolution of the shell it is important to know the values of potential (6) at the event horizons of both the inner and outer metrics, $\rho_{\rm h\,in} = (\rho_{\rm h\,in1}, \rho_{\rm h\,in2}, \rho_{\rm h\,in3})$ and $\rho_{\rm h\,out} = (\rho_{\rm h\,out1}, \rho_{\rm h\,out2}, \rho_{\rm h\,out3})$, respectively. By using equation (2) for the inner event horizon radius, $r = \rho_{\rm h\,in}$, and equation (6) for potential, after some algebraic manipulation we obtain

$$U(\rho_{\rm h\,in}) = -\frac{\left\{2\left[\frac{\varepsilon_{\rm in}m_{\rm out}}{6\pi\sigma^2} - m_{\rm in}(1+\frac{\varepsilon_{\rm out}}{6\pi\sigma^2})\right] + \rho_{\rm h\,in}\left(1+\frac{\varepsilon_{\rm out}-\varepsilon_{\rm in}}{6\pi\sigma^2}\right)\right\}^2}{[8\rho_{\rm h\,in}(\rho_{\rm h\,in}-2m_{\rm in})]} \le 0. \tag{18}$$

Analogously, for the outer event horizon $r = \rho_{\rm h\,out}$ we obtain

$$U(\rho_{\rm h\,out}) = -\frac{\left\{2\left[\frac{\varepsilon_{\rm out}m_{\rm in}}{6\pi\sigma^2} - m_{\rm out}\left(1+\frac{\varepsilon_{\rm in}}{6\pi\sigma^2}\right)\right] + \rho_{\rm h\,out}\left(1+\frac{\varepsilon_{\rm in}-\varepsilon_{\rm out}}{6\pi\sigma^2}\right)\right\}^2}{[8\rho_{\rm h\,out}(\rho_{\rm h\,out}-2m_{\rm out})]} \le 0. \tag{19}$$

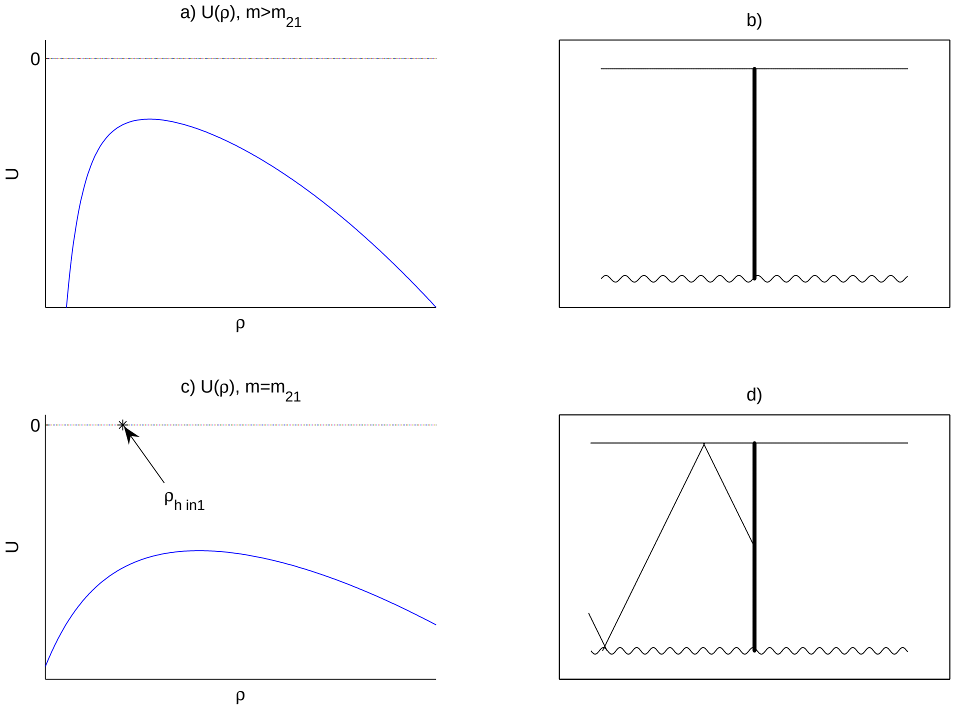

Figure 3. An effective potential (6) and the corresponding Carter-Penrose diagrams for the case $\mu > 0$, $\varepsilon_{\rm out} > \varepsilon_{\rm in} + 6\pi\sigma^2$ and values of the rolling mass parameter m in the range $m > m_{21}$ (graphs a and b) and $m = m_{21}$ (graphs c and d). See Section 3.1 for details.

The equality in (18) and (19) is achieved only at $m = m_1$ (inner metric), where $\rho_{\rm h\,in} = \rho_1$, and, respectively, at $m = m_3$ (outer metric), where $\rho_{\rm h\,out} = \rho_2$. In other words, the points of event horizons of both the inner and outer metrics, $\rho_{\rm h\,in}$ and $\rho_{\rm h\,out}$ cannot be below the potential in the Fig. 2. The gravitational radius $\rho_{\rm h2}$ for both 'in' and 'out' metrics is changed in the range $0 \le \rho_{\rm h2} \le \rho_{\rm h1}$, and, therefore, it is placed at the left of the potential curve. In a similar way, the gravitational radius $\rho_{\rm h3}$ is changed in the range $\rho_{\rm h1} \le \rho_{\rm h3} \le \sqrt{3}\rho_{\rm h1}$, and, therefore, it is placed at the right of the potential curve.

Now we have all necessary ingredients for the investigation of possible motions of the thin vacuum shell in the Schwarzschild-de Sitter metric.

3. Dynamical evolution of vacuum shell

3.1. Case of $\mu > 0$ *and* $\varepsilon_{\rm out} > \varepsilon_{\rm in} + 6\pi\sigma^2$

First of all we consider a simple case, when $\mu > 0$ and $\varepsilon_{\rm out} > \varepsilon_{\rm in} + 6\pi\sigma^2$ (another similar case when $\mu < 0$ and $\varepsilon_{\rm in} > \varepsilon_{\rm out} + 6\pi\sigma^2$ may be analyzed in a similar way). In this case $\sigma_{\rm in} = \sigma_{\rm out} = 1$, as it follows from (7) and (8). Therefore, there are no radii ρ_1 and ρ_2. It can be shown that in this case $m_{21} > m_{22}$, $\rho_{\rm h\,in1} > \rho_{\rm h\,out1}$ and $\rho_{\rm h\,in3} > \rho_{\rm h\,out3}$.

The rolling parameter of our classification scheme is a mass parameter m and we start from the large value of this parameter.

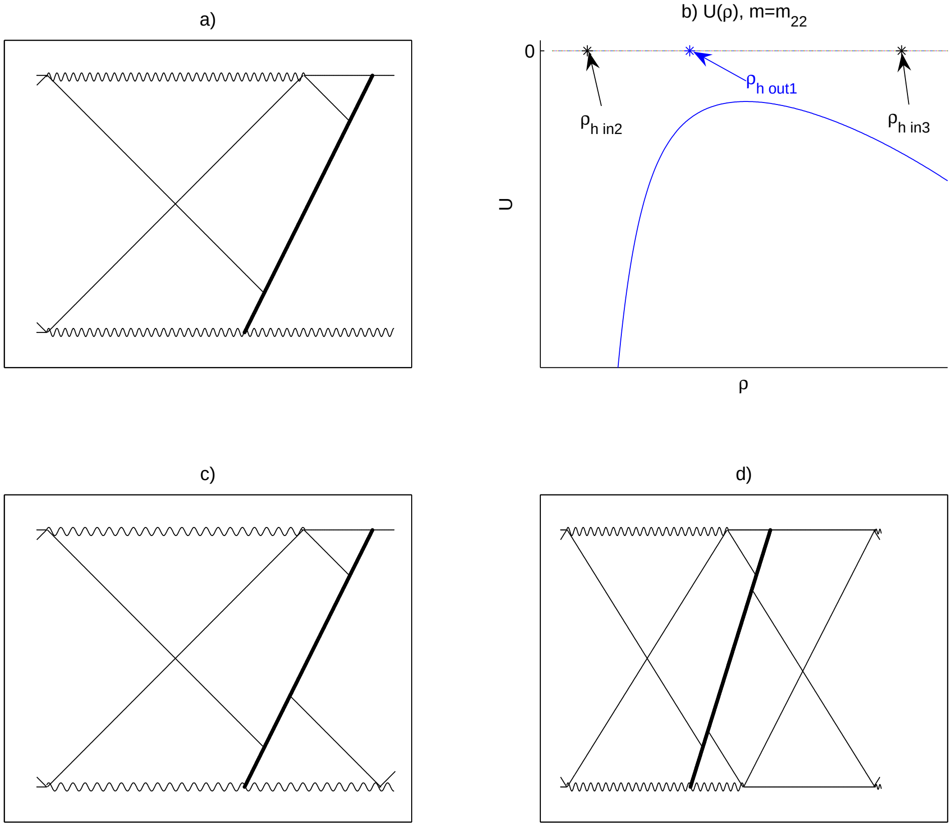

Figure 4. An effective potential (6) and the corresponding Carter-Penrose diagrams for the case $\mu > 0$, $\varepsilon_{\rm out} > \varepsilon_{\rm in} + 6\pi\sigma^2$ and values of the rolling mass parameter m in the range $m_{22} < m < m_{21}$ (graph a), $m = m_{22}$ (graphs b and c) and $m_{22} > m > \max(m_0, m^*)$ (graph d).

If $m > m_{21}$, then an event horizon is absent and initial expansion (or contraction) of the shell is unbounded (there is no bounce point). The corresponding potential $U(\rho)$ and the Carter-Penrose diagram is shown in the Figs. 3a and 3b respectively. Here and further below the Carter-Penrose diagrams are shown only for an initially expanding envelope. The corresponding diagrams for contracting envelope are easily reproduced from the expanding ones by symmetry reflection with respect to the median horizontal line (except for some special cases).

At $m = m_{21}$, the first event horizon appears in the inner metric, $\rho_{\rm h\,in1}$. See Figs. 3c and 3d for the corresponding potential and diagram.

If $m_{22} < m < m_{21}$, then there are two event horizons, $\rho_{\rm h\,in2}$ and $\rho_{\rm h\,in3}$. See Fig. 4a for the Carter-Penrose diagram, while the potential has a similar form as in the previous two cases (Figs. 4a and 3c).

At $m = m_{22}$, the first event horizon appears in the outer metric, $\rho_{\rm h\,out1} < \rho_{\rm h\,in3}$. We prove that $\rho_{\rm h\,in2} < \rho_{\rm h\,out1}$. Indeed, this inequality may be written in the form $(1+\mu)/(1-\mu) > 2\varepsilon_{\rm out}/(3\varepsilon_{\rm out} - \varepsilon_{\rm in})$. For $\mu > 0$, if we will prove the inequality $1 > 2\varepsilon_{\rm out}/(3\varepsilon_{\rm out} - \varepsilon_{\rm in})$, then we prove our statement. The last inequality is evident

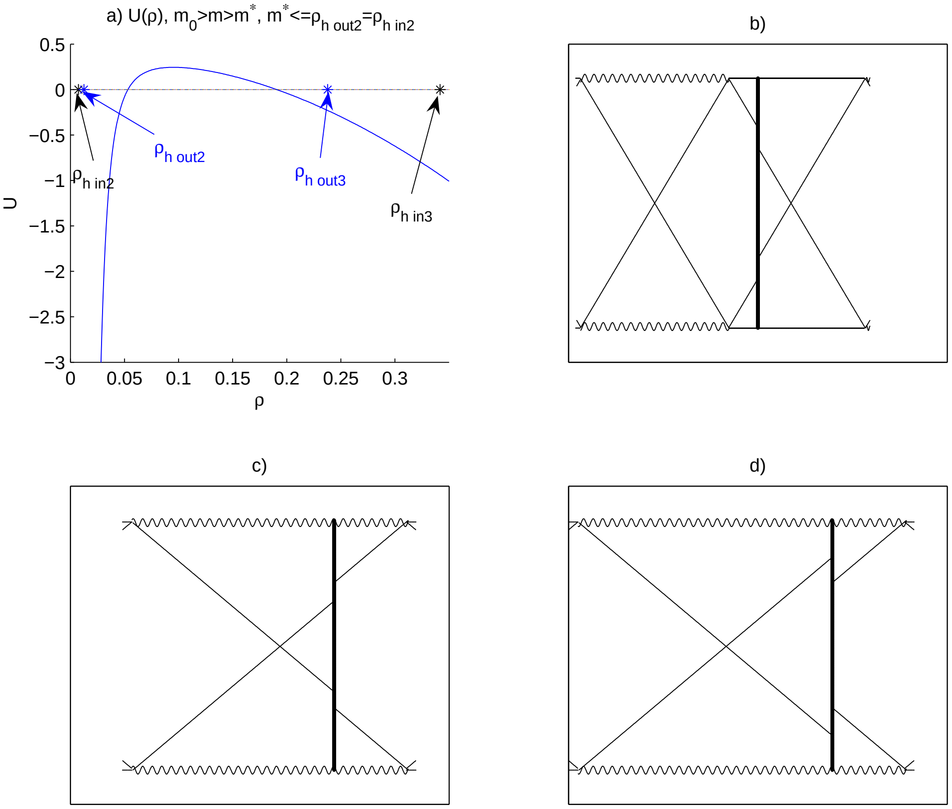

Figure 5. An effective potential (6) and the corresponding Carter-Penrose diagrams for the case $\mu > 0$, $\varepsilon_{\rm out} > \varepsilon_{\rm in} + 6\pi\sigma^2$ and values of the rolling mass parameter m in the range $m < m_0$ (graphs a, b and c), $m^* < m < m_0$ (graphs b and d) and $m < m^* < m_0$ (graphs b and c).

by remembering that $\varepsilon_{\rm out} > \varepsilon_{\rm in} + 6\pi\sigma^2$. So for $m = m_{22}$ the event horizon $\rho_{\rm h\,out1}$ is located between $\rho_{\rm h\,in2}$ and $\rho_{\rm h\,in3}$. See Figs. 4b and 4c for the corresponding potential and the Carter-Penrose diagram of an expanding shell.

If $m_{22} > m > \max(m_0, m^*)$, where m^* is defined from equation $\rho_{\rm h\,in2} = \rho_{\rm h\,out2}$, there are two event horizons, $\rho_{\rm h\,out2}$ and $\rho_{\rm h\,out3}$, in the outer metric. These event horizons are located between the event horizons of the inner metric $\rho_{\rm h\,in2}$ and $\rho_{\rm h\,in3}$. See Fig. 4d for a corresponding diagram.

If $m^* > m_0$ and $m^* > m > m_0$, then the arrangement of event horizons is $\rho_{\rm h\,out2} < \rho_{\rm h\,in2} < \rho_{\rm h\,out3} < \rho_{\rm h\,in3}$. The Carter-Penrose diagram for an expanding shell is shown in the Fig. 8d.

If $m < m_0$, the region appears, where potential $U(\rho)$ is positive (see Fig. 5a). Now solutions for $\rho(\tau)$ have the bounce points. The arrangement of event horizons is $\rho_{\rm h\,out2} < \rho_{\rm h\,in2} < \rho_{\rm h\,out3} < \rho_{\rm h\,in3}$. The Carter-Penrose diagrams for an expanding and contracting shell are shown in the Fig. 5b and Fig. 5c respectively.

If $m_0 > m^*$, then in the case $m^* < m < m_0$ the possible Carter-Penrose diagrams for an expanding and contracting shell are shown in the Figs. 5b and 5d.

In the last case $m < m^*$ the arrangement of event horizons is $\rho_{\rm h\,out2} < \rho_{\rm h\,in2} <$

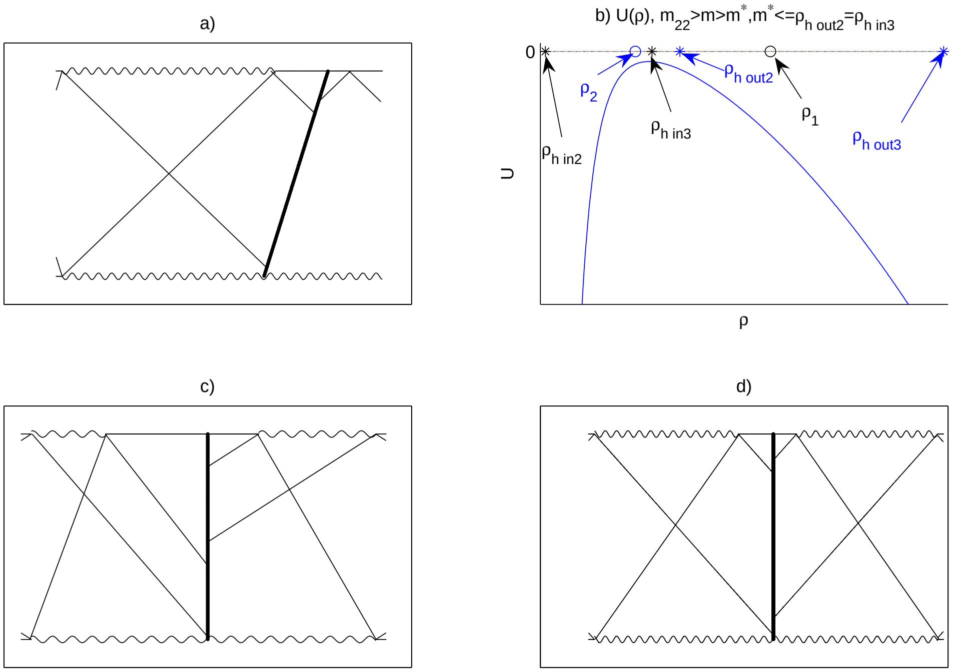

Figure 6. An effective potential (6) and the corresponding Carter-Penrose diagrams for the case $\mu > 0$ and $\varepsilon_{\rm in} > \varepsilon_{\rm out} + 6\pi\sigma^2$ and values of the rolling mass parameter m in the range $m = m_{22}$ (graphs a), $m_{22} > m > m^*$ (graphs b and c) and $m^* > m > m_0$ (graph d).

$\rho_{\rm h\,out3} < \rho_{\rm h\,in3}$. See in the Figs. 5b and 5c the Carter-Penrose diagrams for an expanding and contracting shell respectively. In particular, these diagrams illustrate the formation of a black hole or wormhole after a final contraction of the shell.

3.2. Case of $\mu > 0$ and $\varepsilon_{\rm in} > \varepsilon_{\rm out} + 6\pi\sigma^2$

From this point we start classification of a more tangled case, when $\mu > 0$ and $\varepsilon_{\rm in} > \varepsilon_{\rm out} + 6\pi\sigma^2$ (the case when $\mu < 0$ and $\varepsilon_{\rm out} > \varepsilon_{\rm in} + 6\pi\sigma^2$ may be analyzed in a similar way). Now both $\sigma_{\rm in}$ and $\sigma_{\rm out}$ can change the signs at radii ρ_1 and ρ_2. In the considered case the following inequalities are valid: $\rho_1 > \rho_2$ and $\rho_{\rm h\,out1} > \rho_{\rm h\,in1}$.

It is useful to define the additional 5 dimensionless parameters: $\tilde{\mu}$, $\mu_{\rm out}$, $\mu_{\rm in}$, $\mu_{\rm 1\,out}$ and $\mu_{\rm 1\,in}$. A first parameter is a solution $\mu = \tilde{\mu}$ of the equation $m_{21} = m_{22}$, where

$$\tilde{\mu} = \frac{\sqrt{\varepsilon_{\rm in}} - \sqrt{\varepsilon_{\rm out}}}{\sqrt{\varepsilon_{\rm in}} + \sqrt{\varepsilon_{\rm out}}}. \tag{20}$$

($m_{22} < m_{21}$ at $\mu > \tilde{\mu}$ and vice versa). A second parameter is a solution $\mu = \mu_{\rm out}$ of the equation $\rho_2 = \rho_{\rm h\,out1}$ at $m = m_{22}$, where

$$\mu_{\rm out} = \frac{\varepsilon_{\rm in} - \varepsilon_{\rm out} + 6\pi\sigma^2}{5\varepsilon_{\rm out} - \varepsilon_{\rm in} - 6\pi\sigma^2}. \tag{21}$$

This parameter exists only if $3\varepsilon_{\rm out} > \varepsilon_{\rm in} + 6\pi\sigma^2$. Under this condition $\rho_2 > \rho_{\rm h\,out1}$ at $\mu > \mu_{\rm out}$ and vice versa. In the opposite case, when $3\varepsilon_{\rm out} < \varepsilon_{\rm in} + 6\pi\sigma^2$, it is always

$\rho_2 < \rho_{\rm h\,out1}$. A third parameter is a solution $\mu = \mu_{\rm in}$ of the equation $\rho_1 = \rho_{\rm h\,in1}$ at $m = m_{21}$, where

$$\mu_{\rm in} = \frac{\varepsilon_{\rm in} - \varepsilon_{\rm out} - 6\pi\sigma^2}{5\varepsilon_{\rm in} - \varepsilon_{\rm out} - 6\pi\sigma^2} \tag{22}$$

($\rho_1 > \rho_{\rm h\,in1}$ at $\mu > \mu_{\rm in}$ and vice versa). A fourth parameter is a solution $\mu = \mu_{1\,\rm out}$ of the equation $\rho_{\rm h\,out1} = \rho_{\rm h\,in3}$ at $m = m_{22}$, where

$$\mu_{1\,\rm out} = \frac{\varepsilon_{\rm in} - \varepsilon_{\rm out}}{5\varepsilon_{\rm out} - \varepsilon_{\rm in}}, \tag{23}$$

This parameter exists only if $\varepsilon_{\rm in} < 3\varepsilon_{\rm out}$. Under this condition $\rho_{\rm h\,out1} < \rho_{\rm h\,in3}$ at $\mu > \mu_{1\,out}$ and vise versa. In the opposite case, when $\varepsilon_{\rm in} > 3\varepsilon_{\rm out}$, it is always $\rho_{\rm h\,out1} > \rho_{\rm h\,in3}$. Finally, the fifth parameter is a solution $\mu = \mu_{1\,\rm in}$ of the equation $\rho_{\rm h\,in1} = \rho_{\rm h\,out2}$ at $m = m_{21}$, where

$$\mu_{1\,\rm in} = \frac{\varepsilon_{\rm in} - \varepsilon_{\rm out}}{5\varepsilon_{\rm in} - \varepsilon_{\rm out}} \tag{24}$$

($\rho_{\rm h\,in1} > \rho_{\rm h\,out2}$ at $\mu < \mu_{1\,in}$ and vice versa). It is easy to verify that $\rho_{\rm h\,out1} > \rho_{\rm h\,in2}$ at $m = m_{22}$ and $\rho_{\rm h\,in1} < \rho_{\rm h\,out3}$ at $m = m_{21}$. A mutual arrangement of these 5 parameters is $\mu_{\rm out} > \mu_{1\,out} > \tilde{\mu} > \mu_{1\,in} > \mu_{\rm in}$.

As a first step in classification of the situation, when $\mu > 0$ and $\varepsilon_{\rm in} > \varepsilon_{\rm out} + 6\pi\sigma^2$, we consider the case, when $\mu > \tilde{\mu}$ (the case $\mu < \tilde{\mu}$ is quite a similar). Again we begin from the large value of the rolling parameter m.

If $m > m_{21}$, the event horizons are absent and there are only two radii ρ_1 and ρ_2, where the signs of $\sigma_{in,out}$ are changed. The potential $U(\rho)$ is similar to one shown in the Fig. 3a (where ρ_1 and ρ_2 are not shown). A diagram for an expanding shell is analogous to one shown in the Fig. 3b.

The next case is $m = m_{21}$. Now a first event horizon $\rho_{\rm h\,in1}$ appears, which is at left to ρ_1 (i. e. $\rho_{\rm h\,in1} < \rho_1$). Now potential is similar to one in the Fig. 3c. The crucial point is that now a shell intersects the radius $\rho_{\rm h\,in1}$, when $\sigma_{\rm in} = 1$. The Carter-Penrose diagram is similar to one shown in the Fig. 3d.

If $m_{21} > m > m_{22}$, there are two event horizons $\rho_{\rm h\,in2}$ and $\rho_{\rm h\,in3}$, but qualitatively this case is similar to the preceding one. The Carter-Penrose diagram for an expanding shell is shown in the Fig. 4a.

The case $m = m_{22}$ is divided into subcases. We begin from the subcase $\varepsilon_{\rm in} > 3\varepsilon_{\rm out}$, when inequalities $\rho_{\rm h\,out1} > \rho_{\rm h\,in3}$ and $\rho_{\rm h\,out1} > \rho_2$ are fulfilled. The resulting diagram for an expanding shell is shown in the Fig. 6a. The other subcase will be considered later.

If $m_{22} > m > m^*$, where m^* is a solution of the equation $\rho_{\rm h\,out2} = \rho_{\rm h\,in3}$. Now instead of one event horizon $\rho_{\rm h\,out1}$ there are two event horizons, $\rho_{\rm h\,out2}$ and $\rho_{\rm h\,out3}$. The corresponding potential and the Carter-Penrose diagram are shown in the Fig. 6b and 6c respectively. It must be noted that a moving shell intersects the event horizons $\rho_{\rm h\,out}$ when $\sigma_{\rm out} = -1$. Therefore, a shell intersects these event horizons in the region R_-. On the contrary, a shell intersects the event horizons $\rho_{\rm h\,in}$ in the region R_+ when $\sigma_{\rm in} = 1$.

The only distinguishing feature of the case $m^* > m > m_0$ from the preceding one is swapping round the event horizons $\rho_{\rm h\,out2}$ and $\rho_{\rm h\,in3}$. The arrangement of radii is

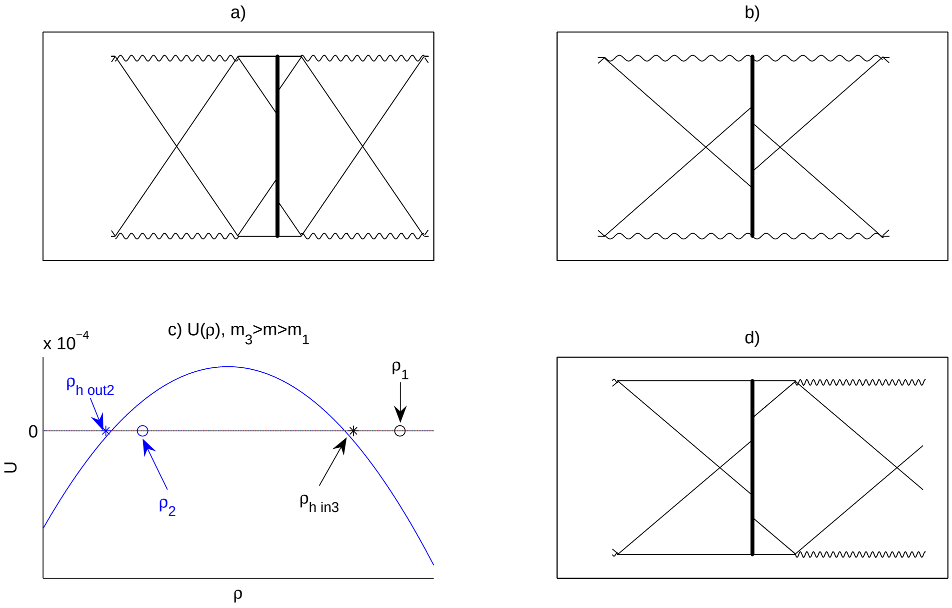

Figure 7. An effective potential (6) and the corresponding Carter-Penrose diagrams for the case $\mu > 0$, $\varepsilon_{\rm out} > \varepsilon_{\rm in} + 6\pi\sigma^2$ and values of the rolling mass parameter m in the range $m_0 > m > m_3$ (graphs a and b), $m_3 > m > m_1$ (graphs c) and $m < m_1$ (graph d).

$(\rho_{\rm h\,in2}, \rho_2) < \rho_{\rm h\,out2} < \rho_{\rm h\,in3} < (\rho_1, \rho_{\rm h\,out3})$. A corresponding diagram is shown in the Fig. 6d.

If $m_0 > m > m_3$, the potential intersects the axis $U = 0$ and a shell will bounce from the potential. The arrangements of radii is the same as in the previous case. The diagrams for expanding and contracting shell are shown in the Fig. 7a and 7b respectively.

If $m_3 > m > m_1$, the radii $\rho_{\rm h\,out2}$ and ρ_2 are swapped round. The potential is shown in the Fig. 7c (the event horizons $\rho_{\rm h\,out3}$ and $\rho_{\rm h\,in2}$ are not shown). A diagram for an expanding shell is the same as in the Fig. 7a. A contracting shell intersects the event horizon $\rho_{\rm h\,out2}$ in the region R_+ (when $\sigma_{\rm out} = 1$). A diagram for a contracting shell is shown in the Fig. 5d.

If $m < m_1$, the radii $\rho_{\rm h\,in3}$ and ρ_1 are swapped round. Two radii $\rho(1)$ and $\rho(2)$ (where signs of $\sigma_{in,out}$ are changed) is now under the potential graph. The diagram for a contracting shell is the same as in the previous case (see Fig. 5d). A corresponding diagram for an expanding shell is shown in the Fig. 7d.

Now we return to another subcase of the case $m = m_{22}$, when $\varepsilon_{\rm in} + 6\pi\sigma^2 > 3\varepsilon_{\rm out} > \varepsilon_{\rm in}$, the inequality $\rho_2 < \rho_{\rm h\,out1}$ is fulfilled and parameter $\mu_{1\,out}$ exists. If $\mu > \mu_{1\,out}$, then $\rho_{\rm h\,out1} < \rho_{\rm h\,in3}$. The arrangement of radii is $(\rho_{\rm h\,in2}, \rho_2) < \rho_{\rm h\,out1} < \rho_{\rm h\,in3} < \rho_1$. A diagram for an expanding shell is shown in the Fig. 8a.

If $m_{22} > m > \max(m_0, m^*)$, where m^* defined from equation $\rho_{\rm h\,in3} = \rho_{\rm h\,out3}$, instead of the one event horizon $\rho_{\rm h\,out1}$ there are two event horizons $\rho_{\rm h\,out2,3}$. The arrangement of radii is $(\rho_{\rm h\,in2}, \rho_2) < \rho_{\rm h\,out2} < \rho_{\rm h\,out3} < \rho_{\rm h\,in3} < \rho_1$. A corresponding diagram for an

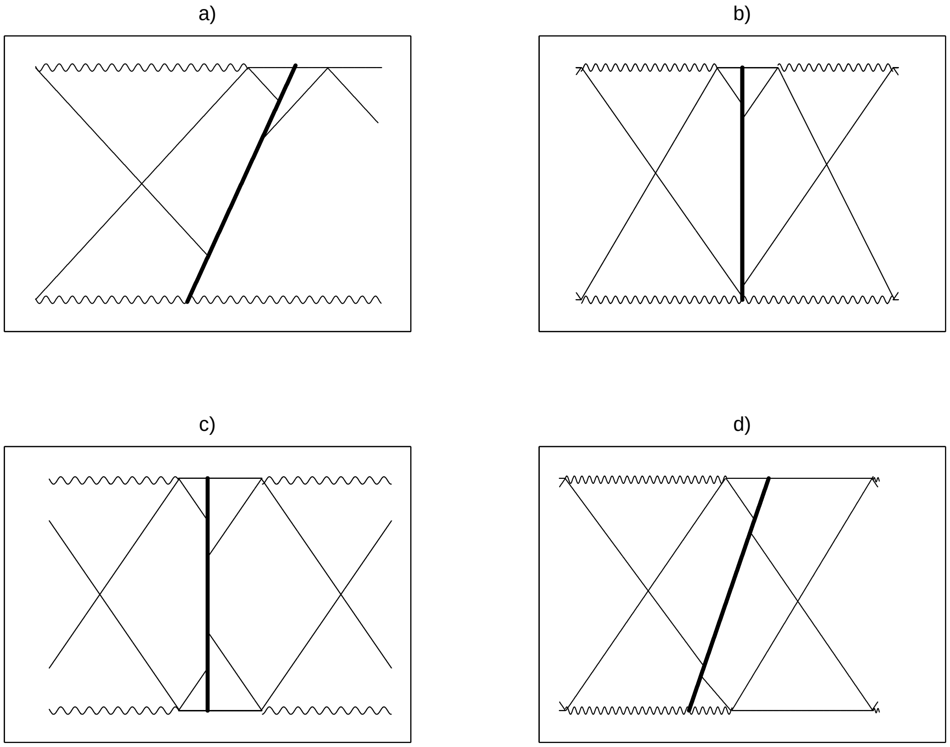

Figure 8. An effective potential (6) and the corresponding Carter-Penrose diagrams for the case $\mu > 0$, $\varepsilon_{\rm out} > \varepsilon_{\rm in} + 6\pi\sigma^2$ and values of the rolling mass parameter m in the range $\mu > \mu_{1\,out}$ and $\mu > \mu_{1\,out}$ (graphs a), $m_{22} > m > \max(m_0, m^*)$ (graphs b) and $m_0 > m > m_3$ (graphs c).

expanding shell is shown in the Fig. 8b.

If $m^* > m > m_0$, the arrangement of radii is $(\rho_{\rm h\,in2}, \rho_2) < \rho_{\rm h\,out2} < \rho_{\rm h\,in3} < (\rho_1, \rho_{\rm h\,out3})$. The only difference with preceding subcase is swapping round the event horizons $\rho_{\rm h\,in3}$ and $\rho_{\rm h\,out3}$. A diagram for an expanding shell shell shown in the Fig. 6d.

If $m_0 > m > m_3$, the potential intersects the axis $U = 0$ and the bounce point appears. The arrangement radii is a similar to the previous case, but a shell now can bounce from the potential. The diagrams for an expanding and contracting shells are shown in the Figs. 7a and the 7b respectively. At $m_0 > m^*$ and at $m_0 > \max(m_3, m^*)$ there will be the following arrangement of radii : $(\rho_{\rm h\,in2}, \rho_2) < \rho_{\rm h\,out2} < \rho_{\rm h\,out3} < \rho_{\rm h\,in3} < \rho_1$. The diagrams for an expanding and contracting shells are shown in the Figs. 8c and 7b respectively. The next two subcases depend on the relation $m_3 \lesseqgtr m^*$ and are described in a similar way. The remaining cases for $m < (m_3, m^*)$ are similar to ones for $\varepsilon_{\rm in} > 3\varepsilon_{\rm out}$.

If $\mu_{1\,out} > \mu > \tilde{\mu}$ in the case $\varepsilon_{\rm in} + 6\pi\sigma^2 > 3\varepsilon_{\rm out} > \varepsilon_{\rm in}$, then $\rho_{\rm h\,out1} > \rho_{\rm h\,in3}$. As a result this case is reduced to the case, when $\varepsilon_{\rm in} > 3\varepsilon_{\rm out}$.

If $3\varepsilon_{\rm out} - 6\pi\sigma^2 > \varepsilon_{\rm in}$ for $m = m_{22}$, then the inequality $\rho_{\rm h\,out2} > \rho_{\rm h\,in2}$ is fulfilled and besides the parameter $\mu_{1\,out}$ there exists also $\mu_{\rm out}$. At $\mu > \mu_{\rm out}$, the inequalities $\rho_{\rm h\,out1} < \rho_{\rm h\,in3,}$ and $\rho_2 > \rho_{\rm h\,out1}$ are valid. As a result the arrangement of radii is

$\rho_{\rm h\,in2} < \rho_{\rm h\,out1} < (\rho_2, \rho_{\rm h\,in3}) < \rho_1$. A corresponding diagram for an expanding shell is shown in the Fig. 4c.

If $m_{22} > m > m_0$, instead of the one event horizon $\rho_{\rm h\,out1}$ there are two event horizons $\rho_{\rm h\,out2}$ and $\rho_{\rm h\,out3}$ and the arrangement of radii is $\rho_{\rm h\,in2} < \rho_{\rm h\,out2} < \rho_{\rm h\,out3} < (\rho_2, \rho_{\rm h\,in3}) < \rho_1$. A corresponding diagram for an expanding shell is shown in the Fig. 4d.

If $m_0 > m > m_3$, the potential intersects the axis $U = 0$ and a shell can bounce from the potential. The corresponding diagrams for an expanding and contracting shells are shown in the Figs. 5b and 5d respectively.

If $m_3 > m > m^*$, where m^* is a solution of the equation $\rho_{\rm h\,out3} = \rho_{\rm h\,in3}$, the event horizon $\rho_{\rm h\,out3}$ changes the place with ρ_2. The coincidence of these radii occurs at the radius, where $U(\rho) = 0$. The radius ρ_2 now is under the potential curve. A shell will intersect $\rho_{\rm h\,out3}$ with $\sigma_{\rm out} = -1$. A corresponding diagram for an expanding shell is shown in the Fig. 8c.

The case $m^* > m$ is similar to one for $\varepsilon_{\rm in} > 3\varepsilon_{\rm out}$. The case $\mu_{\rm out} > \mu > \mu_{1\,out}$ is similar to one for $\varepsilon_{\rm in} + 6\pi\sigma^2 > 3\varepsilon_{\rm out} > \varepsilon_{\rm in}$. Finally, the case $\mu_{1\,out} > \mu > \tilde{\mu}$ is similar to one for $\varepsilon_{\rm in} > 3\varepsilon_{\rm out}$. Analogously is considered the case, when $\tilde{\mu} > \mu > 0$, and the case, when exists only one of the two radii, ρ_1 or ρ_2. This case completes the classification.

4. Conclusion

We classified all possible evolution scenarios of a thin vacuum shell in the Schwarzschild-de Sitter metric and constructed the Carter-Penrose diagrams for corresponding global geometries. These geometries illustrates the possibilities for final formation of black holes and wormholes or eventual expansion of bubbles.

Acknowledgments

We acknowledge Viktor Berezin and Yury Erochenko for helpful discussions. This work was supported in part by the Russian Foundation for Basic Research grants 06-02-16342-a and the Russian Ministry of Science grants LSS 5573.2006.2.

References

[1] Zeldovich Ya B, Kobzarev I Yu and Okun L B 1974 *Zh. Eksp. Teor. Fiz.* **67** 3
[2] Voloshin M B, Kobzarev I Yu and Okun L B 1974 *Sov. Nucl. Phys.* **20** 1229
[3] Coleman S 1977 *Phys. Rev.* D **15** 2929
[4] Callan C G and Coleman S 1977 *Phys. Rev.* D **16**, 1762
[5] Coleman S and De Luccia F 1980 *Phys. Rev.* D **21** 3305
[6] Israel W 1966 *Nuovo Cimento* B **44** 1
[7] Berezin V A, Kuzmin V A and Tkachev I I 1983 *Phys. Lett.* B**120** 91
[8] Berezin V A, Kuzmin V A and Tkachev I I 1985 *Pis'ma Zh. Eksp. Teor. Fiz.* **41** 446
[9] Berezin V A, Kuzmin V A and Tkachev I I 1987 *Sov. Phys.-JETP* **93** 1159
[10] Berezin V A, Kuzmin V A and Tkachev I I 1987 *Phys. Rev.* D **36** 2919
[11] Sato K, Sasaki M, Kodama H and Maeda K 1981 *Prog. Theor. Phys.* **65** 1443

[12] Sato K, Sasaki M, Kodama H and Maeda K 1982 *Phys. Lett.* B **108** 103
[13] Frolov V P, Markov M A and Mukhanov V F 1990 *Phys. Rev.* D **41** 383
[14] Blau S K, Guendelman E I and Guth A H 1987 *Phys. Rev.* D **35** 1747
[15] Aguirre A, Johnson M 2005 *Phys. Rev.* D **72** 103525
[16] Lee B-H, Lee W, Nam S and Park C 2007 *Phys. Rev.* D**75** 103506
[17] Dokuchaev V I and Chernov S V 2007 *Pis'ma Zh. Eksp. Teor. Fiz.* **85** 727
[18] Aurilia A, Palmer M, and Spallucci E 1989 *Phys. Rev.* D **40** 2511
[19] Aguirre A, Johnson M C 2006 *Phys. Rev.* D **73** 123529, ArXiv:gr-qc/0512034
[20] Chao Wu Zhong 1983 *Phys. Rev.* D **28** 1898
[21] Aurilia A, Denardo G, Legovivni F and Spallucci E 1984 *Phys. Lett.* B **147** 258
[22] Alberghi G L, Lowe D A and Trodden M 1999 *J. High Energy Phys.* JHEP07(1999)020
[23] Goncalves M C V 2002 *Phys. Rev.* D **66** 084021